Agave Sisalana for distributed production of absorbent media for menstrual pads in semi-arid regions

April 20, 2023

Anton Molina[1,2,†], Anesta Kothari[2,†], Alex Odundo[3], Manu Prakash[2*]

[1]Department of Materials Science and Engineering, [2]Department of Bioengineering

Stanford University, 450 Serra Mall, Stanford, California 94305

[3]Olex TechnoEnterprises, Kisumu, Kenya

[*]To whom correspondence should be addressed; E-mail: manup@stanford.edu

[†] These authors contributed equally

Abstract

Agaves are robust, draught tolerant plants that have been cultivated for their high-strength fibers for centuries and they hold great promise as a crop in the face of increasing water scarcity associated with a warming planet. Meanwhile, millions of women lack access to sanitary products to safely manage their menstruation particularly in low- and middle-income countries characterized by a dry climate. To address this issue, we show a processing route that transforms the leaves of the succulent Agave sisalana into a highly absorbent and retentive (23 g/g) material. The process involves delignification combined with mechanical fluffing to increase affinity for water and porosity, respectively. This process leads to a material with an absorption capacity exceeding those found in commercially available products such as menstrual pads. Finally, the carbon footprint water usage associated with this process is comparable with common alternatives with the added benefit that it can be carried out at small scales while remaining environmentally sustainable. Our work represents a step towards distributed manufacturing of essential health and hygiene products based on a local bioeconomy.

Introduction

Absorption materials are critical for a variety of items essential to basic quality of life such as bandages, diapers, and menstrual hygiene products. There is a large gap in the availability of menstrual hygiene products across the world. It is estimated that nearly 500 million women lack access to menstrual hygiene products [1]. In the absence of appropriate solutions such as disposable sanitary napkins, menstruating women often resort to improvised solutions which may pose a health risk or are forced into non-participation which results in unequal economic outcomes [2]. These negative outcomes associated with inadequate means to manage menstruation are often referred to as 'period poverty' [3]. The use of improvised solutions such as cloth rags are particularly prevalent in rural settings (Fig. 1a) [4], where imported products are unable to achieve last mile distribution or are otherwise prohibitively expensive [1] (Supplementary Note 1, Supplementary Fig. 1).

Local manufacturing of disposable menstrual pads is emerging as a promising route for addressing short-comings associated with relying on imported products, especially in serving the needs of rural communities [5]. However, these entities are often challenged by access to quality raw materials [6, 7]. This challenge can be compounded by local climate, for example water intensive production in semi-arid climates [8, 9]. At the same time, many conventional disposable menstrual pads represent a significant sustainability challenge in terms of plastic waste [10, 11], health effects [12], and their burden on sanitation systems [1, 13].

The key functional material in the vast majority of disposable menstrual pads is a fluff pulp composed of cellulosic fibers derived from wood. In general, wood resources are regarded as a promising, renewable replacement for many petroleum-based products [14]. However, wood resources are distributed unequally across the planet (Fig. 1b) [15]. Furthermore, wood fibers are extracted from chips using a harsh chemical treatment known as the Kraft process [16]. This process can only be implemented in an economically and environmentally sustainable manner with extremely high material throughput (400-1500 kton/year) [17]. This combination of unequally distributed resources manufactured in a large-scale, centralized manner introduces supply chain fragility and leads to unequal access to downstream products [18, 19]. Non-wood feedstocks have long been considered as alternative feedstocks for the pulp and paper industry. However, challenges associated with consistent feedstock supply, higher cost of transport due to low density, and the need to adjust the Kraft chemistry due to different chemical compositions of the feedstocks have hindered adoption at large scales [20, 21]. In support of these efforts, comparative studies of non-wood biomass have focused on properties predictive of performance in paper making [22, 23] while properties relevant for niche applications such as absorption have remained largely unexplored [24, 25]. Nonetheless, small-scale pulping of non-wood alternatives have found application as absorbent materials for use in the production of

disposable menstrual pads by small and medium sized entities [7]. While many of these efforts have struggled to scale and suffer from inconsistent or poor quality, they have demonstrated that meaningful social and environmental impact can be made by these emerging "micro pulping" facilities ($\sim$ 1 ton/year) [1, 26, 7, 12].

Biology provides us with examples of efficient delignification operating at the organismic scale. Wood-eating termites and wood-rot fungi represent "powerful mills that reduce ligneous food to a pulpy condition" [27]. While the mechanisms by which these systems operate are not fully understood, biological delignification is a multi-enzymatic process mediated [28] by diffusible small molecules [29]. The separation of cellulose from the lignin-rich binding matrix does not require complete degradation of the lignin. Non-enzymatic processes such as Fenton chemistry might be sufficient to disrupt crosslinks between cellulosic fibers and the lignin-rich binding matrix [30]. Recently, this chemistry has been applied to biorefining [31], wastewater treatment [32, 33], and as a chlorine-free alternative to bleaching in the pulp and paper industry [34]. In particular, the decomposition of organic peracids into reactive carbon-centered radicals enables an increased reactivity towards organic material compared to inorganic peroxides [35, 36]. In the case of peroxyformic acid, decomposition occurs rapidly into water and carbon dioxide, eliminating the introduction of adsorbable organic halides into the environment [37]. Meanwhile synthetic systems that allow for recycling of reagents have also emerged based on solid di-carboxylic acids [38], deep eutectic solvents [39], and organosolv pulping [40, 23]. Thus, there are two conceptual approaches to operating the pulping process that minimize dependence on an external chemical supply chain: recycling and on-site production. If the reagents can be recycled, energy must be expended to recover them. If reagents are consumed, then they must be efficiently produced on-site. Our study is motivated by the increasing capacity for on-site production of chemicals like formic acid [41, 33] and hydrogen peroxide [42, 43, 44]. Few studies have investigated the use of these technologies to implement a bioinspired strategy to transform lignocellulosic biomass into absorbent media in an environmentally sustainable way at small scales.

To date, most local pad manufacturing efforts are built around the use of a limited number of plants, with banana pseudostems being one of the most common [45, 46]. However, a reliance on a small number of plants reduces the ability of this type of manufacturing to extend into different geographies with distinct biomes. With this in mind, *Agave sisalana* (Sisal) is a promising candidate. Sisal is an extremely robust and drought tolerant plant [47] traditionally used in the manufacture of cordage due to its strength and durability. Despite these attractive features, global production has been in decline since the introduction of synthetic fibers [48, 49]. However, it has received renewed attention for its hardiness and potential to serve as a commodity crop in dry climates or on otherwise marginal lands. The biological basis for its success is rooted in the plant's crassulacean metabolism (CAM) [50]. While nearly 7 % of all plants use the CAM mechanism, the majority of them are small and lack any obvious economic value. Even though sisal

4

has been used as a fiber feedstock in semi-arid regions for centuries, current applications remain limited. Expanding our capacity for obtaining useful materials from draught resistant commodity crops is critical for adapting to a warming planet and associated changes in biomass distribution. To our knowledge, an efficient demonstration of fiber extraction and use in absorbent applications has not been demonstrated.

Here, we apply a mild delignification chemistry based on peroxyformic acid to obtain absorbent microfibers from sisal that exceed the performance of cotton from commercially-available menstrual pads (cotton-CMP). We characterize the physical and chemical properties to understand structure-function relationships across multiple length scales. Finally, we perform a carbon and water footprint analysis of the manufacturing process and compare it with common alternatives showing that this strategy represents a route towards reductions in greenhouse gas emissions. These results represent a sustainable solution for providing access to high-quality absorption materials in semi-arid regions to enable local downstream production of sanitary napkins and other personal hygiene products. By developing a strategy for responsible manufacture of products aimed at reducing gender inequality, our work addresses several of the 17 Sustainable Development Goals described by the United Nations.

Results and discussion

Design criteria and evaluation

A few criteria must be satisfied in order to obtain an absorbent and retentive material from a disordered network of fibers. In general, the maximum absorption capacity of a porous media is a function of its porosity ϕ:

$$A = \frac{\rho_l}{\rho} \frac{\phi}{1 - \phi} \tag{1}$$

where ρ_l is the density of the absorbed liquid and ρ is the density of the material from which the absorbent media is composed [51]. However, porosity alone is not sufficient. The material must also imbibe and retain liquid. The Lucas-Washburn equation can describe the ability of porous media to imbibe liquid by considering capillary flow in a bundle of cylindrical tubes. The penetration length L of a liquid with surface tension γ and dynamic viscosity η is a function of time given by:

$$L(t) = \sqrt{\frac{\gamma r cos(\theta)}{2\eta}} t^{1/2} \tag{2}$$

where θ is the contact angle between the imbibed liquid and the solid and r is the pore radius. This analysis

5

shows that the desired material will require a low contact angle. The role of pore size is more complicated, since larger pores will allow for fast mass flux as indicated by the Washburn equation while smaller pores will allow for a greater capillary pressure and will likely be associated with a higher surface area. A greater hydrophilic surface area will help the material retain the imbibed fluid when subject to an external load, a common scenario for most applications. Thus, the material must have a low contact angle, high porosity, and a significant fraction of small pores.

To accommodate this complexity in geometry and chemistry, we use absorption of a viscous test liquid under an applied load as a means for evaluating materials produced from biomass following the SCAN-C-33-80 standard (Supplementary Video 2) [24]. Fibers are compressed into a template with area 3.175 mm^2. Specimen height is often sensitive to how the specimen is dried. The viscous test solution is composed of a mixture of glycerol and water. This solution is designed to mimic the rheological properties of blood and was prepared according to IS 5405:1980 (Supplementary Note 2, Supplementary Fig. 2) [52]. Key performance results from this study are shown in Fig. 1k, showing that materials derived from sisal can meet and exceed the performance of cotton-CMP. What follows characterizes the physical and chemical transformations that underlie the conversion of sisal leaves into a highly absorbent material.

Delignification of sisal fibers

A challenge in working with non-wood feedstocks is that the properties of the fiber depend not only on the growing conditions but also on how the fibers have been harvested and subsequently extracted from the surrounding plant tissue primarily composed of parenchymal cells. For example, depending on the nature of the tissue, fibers can be extracted mechanically [53] through decortication (Fig 1d, Supplementary Fig. 3) or enzymatically by retting [54]. Furthermore, care must be taken during decortication [55] to ensure that structural defects (e.g. kinks) do not accumulate on the fibers which might affect downstream absorption properties [25]. What's left are hierarchically-structured, lignin-rich macrofibers fibers held together by an amorphous binding matrix composed of lignin, hemicellulose, and proteins such as pectin (Fig. 1g). In order to be useful in absorbent applications, a substantial fraction of the hydrophobic lignin must separated from the hydrophilic, cellulosic fibers in order to ensure uptake and retention of liquid. We begin by demonstrating that absorbent media cannot be obtained from sisal subject to mild soda pulping conditions. The resulting fibers show only a slight increase in absorption capacity (Figure 1k, Supplementary Note 3).

In order to efficiently separate the cellulosic fibers from the lignin rich binding matrix, we first treat the fibers with *in situ* prepared peroxyformic acid (50°C) followed by an alkali wash (50°C) (Supplementary Video 3) [56, 57]. Treatment with a peroxyformic acid solution can be regarded as a mild delignification

which selectively removes lignin while preserving the structure of the cellulose microfibers. As noted in earlier work, this process is considerably less energy intensive than conventional delignification procedures which occur at high temperatures (80-160°C) and pressures (for example, $\geq$ 0.5 MPa). The acidic conditions provided by the presence of aqueous formic acid will allow for hydrolysis of ether linkages leading to a reduced molecular weight of lignin and increased solubility [58, 59]. Additionally, under acidic conditions, peroxides and peracids are powerful oxidizing agents that react electrophilically with electron-rich aromatic and olefinic structures [60] to produce carboxylic acids.

Following the oxidation with an organic peracid under acidic conditions, an extended sodium hydroxide wash acts to solubilize the cleaved and carboxylated lignin fragments. Meanwhile, hemicelluloses are generally regarded as soluble under alkali conditions where hydroxyl radicals can interrupt the hydrogen bonding of these branched polymers [61]. The exact details of the reaction pathways are difficult to know and are out of the scope of the present research, since they depend on both the identity of the reactive oxygen species and the composition of the lignins involved. High concentrations (10%) of peroxyformic acid yield sisal microfibers that appear completely bleached with a yield of 60% (w/w) (Supplementary Fig. 5). Lower concentrations (1%) of peroxyformic acid yield microfibers that retain some brown color, suggesting the presence of lignin chromophores on fiber surface (Supplementary Fig. 6). Despite the presence of some residual lignin, the absorption performance, while reduced compared with the totally delignified samples, is still competitive with cotton-CMP (Fig. 1k).

To test our understanding of what is happening during each step, we characterize the structural and chemical properties of the resulting fibers using scanning electron microscopy (SEM) (Fig. 2b-d) and Fourier transform infrared attenuated total reflection (FTIR-ATR) spectroscopy (Fig. 2h), respectively. We see that unprocessed sisal fibers are large with diameters $/eq$ 100-250 μm (Figure 2b). These large fibers are characterized by a rough surface in part due to debris from parenchymal cells [62]. Following treatment with the pexoyformic acid solution, we observe the macrofibers beginning to debundle into their smaller constituents (Fig. 2c). Debundling occurs along both the radial and axial dimensions of the fibers. This suggests that the polymers composing the binding matrix have undergone cleavage. However, we also observe a surface roughness which we attributed to residue from the material (lignin, hemicellulose, and proteins) binding these fibers into these larger bundles. FTIR spectra show the elimination of the peaks at 1240 and 1510 cm^{-1}. These peaks correspond to C-O, C-C stretch and aromatic ring vibrations in lignin, respectively [63]. The removal of these peaks is evidence for hydrolysis of ether linkages and oxidative ring openings in lignin. However, the observed surface roughness suggests that much of the lignin has not yet been solubilized. Finally, following the sodium hydroxide wash step and after mechanical agitation during washing, we see significant debundling of the macrofibers into their constituent microfibers (Fig. 2d). Close inspection of the

7

microfibers shows that they have a smooth surface, suggesting that the lignin composing the binding matrix has been solubilized under alkali conditions. In particular, reactive oxygen species during treatment with peroxyformic acid generate carboxylic acids as a result of oxidative ring opening which then become highly soluble in alkaline solution. This interpretation is supported by the elimination of the peak at 1730 cm^{-1} corresponding to C=O carbonyl stretching mode [64]. Cotton is used as a reference since its composition is nearly pure cellulose [65]. Comparison with cotton-CMP shows that our resulting material closely resembles cellulose.

In order to gain insight into how these different treatment steps affect the wetting properties of the fibers, we performed static angle tensiometry using the Wilhelmy principle which relates wettability W to contact angle according to $W = {cos(\theta)}/{\gamma}$, where θ is the contact angle and γ is the surface tension of water and wettability is the force of the submerged fiber (F) normalized by the fiber perimeter (P) (Fig. 2i), Supplementary Figure 7) [66]. Measurement of boiled sisal showed moderately hydrophilic material with contact angle of 46° whereas treatment with peroxyformic acid and sodium hydroxide gave contact angles 32° and 24°, respectively. The contact angle of alkali treated fibers are equivalent to the contact angle obtained from cotton-CMP, providing confirmation of the FTIR analysis that the chemical properties of the sisal microfibers is nearly pure cellulose. While contact angle measurements of natural fibers do have severe limitations as described in the literature [67], these results indicate a progressive increase in the hydrophilicity of the fiber surface with each step.

With a reduction in contact angle, we would expect an increasing trend in absorption for samples prepared from the treated materials (Figure 2j). This idea was tested by preparing samples from material after each treatment step and letting them air dry. Interestingly, there is not a significant increase in absorption following treatment with peroxyformic acid alone. However, there is an appreciable increase following alkali treatment. At this point, there is still a significant gap between the alkali treated samples and the performance of cotton-CMP despite very similar physical and chemical properties of individual fibers.

Structure of fluff pulp materials

The capacity of a fibrous material to absorb and retain liquid depends not just on the properties of individual fibers but also on their mesoscale structure. Porosity and pore size distribution are generally regarded as key structural factors at the network scale which determine absorption performance[51]. The relationship described in Equation 1 suggests that to increase absorption capacity, increasing porosity will be key. However, the challenge in producing porous materials from wet fiber building blocks is network collapse and

8

fiber-fiber bonding due to capillary forces generated during evaporation causing a reduction in porosity and non-trivial changes in the pore size distribution (Fig. 3a).

There are two strategies to obtain highly porous materials from wet fibers. The first is to eliminate capillarity during drying. This can be realized by freeze drying, that is to replace evaporation with sublimation. The second is to disrupt any structures that do form through a mechanical process like blending, milling, or pulverizing (Fig. 3a). The later is practiced industrially using a hammermill where chemical debonding and anti-static agents are added to reduce energy costs and increase yields. Here, we compare the performance of samples prepared by freeze drying with blending implemented using a benchtop blender without the use of any chemical agents (Fig. 3c). We can see that blending substantially increases the absorption capacity of the materials resulting in an increase from 9.64 g/g to 23.94 g/g. To verify that porosity is a key control parameter in this process, we plot absorption for all of the samples prepared as a function of porosity (Fig. 3 d). In general, good agreement with Equation 1 speaks to the high capacity for liquid retention since the curve represents the theoretical maximum for a liquid with $\rho_l = 1.08 \ g/mL$.

Since the effectiveness of these bulk processing steps is driven by microstructural changes, we acquired X-ray computer microtomography (μCT) images of samples before (Figure 3k) and after dry blending (Figure 3 l, m) at the millimeter scale. Analysis of the unblended samples shows a significant amount of macrofibers with diameters $\sim 100 \ \mu m$ dispersed in a random matrix of microfibers ($\sim 20 \ \mu m$). We suspect some fraction of these fiber bundles exist after the peroxyformic acid treatment; however, their extent might also be increased by capillary adhesion. In contrast, these bundles are entirely eliminated following dry blending. The dry blended samples consists of an isotropic distribution of single microfibers. We also observe that this is accompanied by narrowing of the pore size distribution with the average shifted towards smaller pores, satisfying the criteria for a highly absorbent material.

Comparison with other potential lignocellulosic feedstocks

To see whether or not this process can be readily extended to other potentially abundant sources of lignocellulosic biomass, we apply this procedure to flax and hemp fibers (Fig. 4). At the macroscale, we observe that all samples have been converted to a white fibrous material. There is a clear difference in porosity between the two materials with flax-derived fluff pulp being much denser than the hemp-derived fluff pulp and both, in turn, being less dense than cotton-CMP. Comparison of structural features from SEM images of individual fibers before (Fig. 4 d and e) and after (Fig. 4f, g) processing show similar debundling through delignification occurring for both fiber types. Both display an increased rough surface attributed to a second layer of debundling, exposing 1 μm fibers. These features could pin the advancing contact line and reduce

the uptake of fluid into the porous media. Further, we observe that flax fibers consist primarily of short, kinked fibers. We suspect that shorter fibers can pack more densely, resulting in a less porous and therefore less absorbent material. FTIR characterization shows that the processing converts lignified material with distinct spectra into a material with similar functional group composition as cotton-CMP (Fig. 4j). Despite these functional group similarities, measurement of absorption performance follows the trend in density. While both flax and hemp underperform cotton-CMP and sisal, their performance does not preclude their use in absorbent applications. Taken together, these observations suggest that structural features at the single fiber level can play a decisive role in determining the performance of the resulting material.

Life cycle carbon footprint analysis

The unique biological characteristics of sisal make it and other members of the agave family promising candidates for building a bio-economy. Sisal can be harvested year round in across a variety of geographies (Fig. 5a) yielding of over 200,000 tonnes globally in 2020 [68]. Sisal is planted at densities of up to 3000-5000 plants per hectare and require 40-48 months before its leaves can first be harvested, after which a total of 50-60 leaves may be collected per year [69] . A typical leaf will contain 4% fibers by weight [70] and the plant will yield leaves until it is 9-12 years old [69, 70]. *Agave sisalana* can yield 1.5 ton/hectare (whole leaf) whereas sisal hybrid 11648 (a cross can be harvested earlier and yield up to 2-3 ton/hectare (whole leaf)[49]. Meanwhile, other members of the agave family shown even higher yields [47]. These figures show that sisal can be cultivated in large enough quantities to support the manufacture of consumer products in semi-arid regions. As a concrete demonstration, we incorporate sisal cellulose fluff pulp into a menstrual pad, borrowing top and bottom layers from a CMP (Figure 5b-d).

To quantify the sustainability of this approach, we perform a cradle-to-gate carbon footprint life cycle analysis (LCA) to determine the impact of sisal cellulose microfiber production (Fig. 5e-g, Supplementary Note 4). The functional unit is 1 kg of sisal cellulose fluff pulp and the system boundaries include sisal cultivation, harvesting, manufacturing, and transportation. The life cycle inventory is shown in Supplementary Tables 1-2. Here, we consider two scenarios: 1) production of sisal as it occurs in the lab and 2) an aspirational scenario where formic acid and hydrogen peroxide are produced on-site using commercially available electrocatalytic systems powered by renewable, solar energy [42, 71]. Our analysis shows that that there is a footprint of 1.195 and 3.475 kg CO2-eq per kg sisal cellulose microfibers for the on-site and lab-scale production scenarios, respectively (Fig. 5f). This is comparable with reported values for the production of bleached cellulose fluff pulp derived from softwood timber resources (0.513-1.113 kg CO2-eq) and from bleached cotton (1.65-5.25 kg CO2-eq) (Supplementary Note 4).

10

Next, we show the carbon footprint associated with each production activity (Fig. 5g, Supplementary Note 5, Supplementary Tables 3-5). We see that the on-site scenario enables significant reduction in the carbon footprint when powered by renewable energy. Further, this footprint compares favorably with competing alternative processes, especially cotton. The large footprint associated with cotton is associated with the amount of energy needed for upstream fertilizer production that is not required in significant amounts by sisal or timber. This highlights the importance of considering the nature of the biomass feedstock in the production production of bio-based materials.

Since this work is motivated by small scale manufacturing efforts producing valuable products from biomass based value chain close to the point of use, we evaluate the transportation of materials after the gate of production (post-gate). More specifically, this means accounting for transportation of the fluff pulp from the fluff pulp processing facility to the pad manufacturing facility and transportation of the assembled product to the final market (Supplementary Note 6, Supplementary Tables 6-8). We neglect last mile distribution due to a paucity of high-quality information, despite it being well known as a significant contributor of cost and greenhouse gas emissions][72]. For the different extended transportation scenarios considered, we find that transportation post-gate accounts for $\sim$5-90% of the total carbon footprint. Again, these are conservative figures since they ignore last mile distribution. Thus, manufacturing built on localized supply chains has the potential to significantly reduce this category of emissions.

In addition to carbon footprint analysis, we compare the direct water consumption for the process described in this work to water consumption of alternatives (Fig. 5h, Supplementary Note 7, Supplementary Table 9). The lab process is competitive in terms of total water consumption (44.6-119.6 kg H20 per kg fluff pulp) while the on-site production scenario requires an additional kg H_2O associated with on-site production of reagents (64.5-139.5 kg H20 per kg fluff pulp). The lower limit makes some conservatives assumptions about water reuse while the upper limit assumes no recycling. While this is more than the water used in the production of softwood-derived fluff pulp which requires 61.78 kg H20 per kg fluff pulp[34, 16], our process avoids the emission of adsorbable organic halides. Compared with water consumption data reported for small-scale production facility located in Uganda, (90-300 kg H_2O per kg absorbent) [7], our process represents a significant improvement. The amount of water consumed can be collected in semi-arid regions (250-500 mm rainfall/y), representing a required catchment area of 610-882 m^2 (Fig. 5i, Supplementary Note 8). This analysis supports the feasibility of fluff pulp production in semi-arid regions.

11

Discussion and conclusions

This study made use of peroxyformic acid chemistry as a route towards extracting absorbent cellulosic microfibers from harvest sisal leaves. In general, peracid chemistry remains largely unexplored, even more so its application in delignification. The observation that partial delignification still results in good absorption and retention suggests that we can expect significant improvement in reagent consumption by controlling peracid concentrations and its activation. Meanwhile extraction of cellulose from lignocellulosic biomass generates a lignin-rich waste stream where the properties of the lignin are sensitive to the extraction chemistry. Developing strategies to valorize these wastestreams will be important since they might enable the production of additional products. For example, waste lignin might be useful for producing compostable barrier sheets [39] while other components might be useful as fertilizer [70]. The former will enable the production of complete products such as menstrual pads using regionalized biomass while the later enables a regenerative bioeconomy [73]. More broadly, this is a chemical strategy that exists amongst many other possible alternatives such as recyclable chemicals, solid di-carboxylic acids, and enzymes. However, understanding these numerous trade offs must be considered within a comprehensive technoeconomic framework.

Despite similarities in functional group composition, the effectiveness of a given biomass feedstock varies significantly depending on its structure. A better understanding of the relationship between biomass structure and processing is clearly needed. The complexity of these relationships highlights the importance of studying the connection between structure and performance in relatively niche applications such as absorption. A deeper understanding of these connections will enable the identification of lignocellulosic fiber feedstocks that are amenable to this processing strategy. When combined with an understanding of the geospatial distribution of biomass cultivation [74], this knowledge will enable similar production processes to be implemented in distinct climates and biomes.

[deeper understanding of availability of bio resources, previous work on bio-energy supply chains]

Addressing the supply-side problem of period poverty requires innovation in materials and manufacturing methods [1]. Satisfying the growing demand for disposable menstrual pads with conventionally produced products represents a waste and sanitation burden. Existing manufacturing methods and associated supply chains have not succeeded in serving a large fraction of the planet's population, particularly those in rural low- and middle-income settings. Emerging small and medium scale manufacturers producing compostable menstrual pads from locally sourced biomass is an emerging production mode that addresses both concerns of environmental sustainability and product accessibility. In this work, we have shown that organic peracid chemistry can be employed for the partial delignification of sisal fibers to produce an absorbent material with a performance meeting and exceeding that of cotton-CMP. Furthermore, the carbon footprint of this process

12

is competitive with conventional approaches particularly when manufacturing and product distribution exist within the same geographic scope. More broadly, with an increasing demand on timber resources driven by the transition towards the bio-economy, accessing lignocellulosic biomass from alternative sources particularly on dry or otherwise marginal lands will be increasingly important. Our work presents new manufacturing strategies for essential products to be made in a distributed fashion, bringing further economic development in regions disadvantaged by climate.

Materials and Methods

Materials

Sisal leaves were obtained by Alex Odundo in Kisumu, Kenya. Hydrogen peroxide, formic acid, sodium hydroxide, sulfuric acid, iron sulfate, methyl paraben, methylene blue, potassium iodide, glycerol, and ethanol were obtained from Sigma Aldrich and used without further modification. Gum arabic was obtained from Earthborn Elements.

Decortication of sisal leaves

In this work, sisal plants were obtained from the Nyanza region in Kenya . Sisal leaves (Fig.1c and e) were harvested by hand before the fibers were extracted by decortication using a single-head decorticator(Olex Technoenterprises) (Fig. 1d, Supplementary Video 1). The fibers are then cleaned and air dried (Fig. 1f Supplementary Fig. 3). In the dried state, fibers are shelf stable for at least 1 year.

Preparation of sisal cellulose microfibers

Fibers are cut into short segments ($\sim$ 10 mm long) and boiled in water to remove any water soluble components. Following the procedure described Li et al. [57], the stems were then delignified using 10% v/v peroxyformic acid (synthesized in situ by combining 30% hydrogen peroxide with 95% formic acid in a $1:1$ mole-to-mole ratio using 1% sulfuric acid as a catalyst) at 50°C overnight. The fibers were then treated with 4% (w/v) sodium hydroxide for 2 hours at 50°C. In another realization, we followed the procedure describe by Haverty, et al. [31]: cut fibers were delignified using 1% (v/v) peroxyformic acid. In this instance, the amount of sulfuric acid was increased to 4%. The mixture was left to react for 45 mins before adding 400 μL of a solution containing $Fe_2(SO_4)_3$ (1 kg/L). This mixture was then left to react overnight at 50°C overnight. The fibers were then treated with 4% (w/v) sodium hydroxide overnight at 50°C. Finally, the

fibers were washed with three times with equivalent volumes of deionized water or until the pH was neutral. It is important to note that the fibers were subject to approximately of 30 s of vigorous shaking during each wash. This introduction of mechanical energy is analogous to the use of Hollander beater used in conventional paper making and is important for defibrillating the fibers 100 μm macrofiber bundles into smaller microfibers (in the form of wet pulp).

Preparation of test squares

For each test square, a standard acrylic template measuring 1.25"x1.25"x0.25", was used (Supplementary Fig. 2). Three methods were performed to produce various test square samples: (1) freeze drying, (2) air drying without blending, and (3) air drying with blending. For the freeze-dried samples, wet pulp was molded into the acrylic template and frozen at -80° C overnight. The frozen samples were then transferred into a lyophilizer machine (7751000 Freeze Dry System, Labconco) and left to lyophilize over 2 days. For the air dried samples without blending, wet pulp was molded into the acrylic template and left to air dry for 3 days. For the air dried samples with blending, wet pulp was poured onto a mesh surface and left to dry for 3 days. The resulting fluff board was then cut into small pieces ($\sim$1" squares) and dry blended using a benchtop blender (700G Waring Blender). The resulting fluff pulp was then molded into the acrylic template. Each sample was then removed from the template prior to the absorption testing.

Absorption under pressure testing

Absorption is assessed using a test solution prepared according to Indian Standard 5405:1980 [52]. Prior to the absorption test, each test square was weighed (W_i) and its average height measured using a caliper. The absorption under pressure (AUP) setup consists of a liquid bath, a porous transfer plate, a test square sample, a porous transfer plate, and a weight, as shown in (Supplementary Fig. 2). For each AUP, one test square was placed onto the first transfer plate, ensuring it makes contact with the liquid, before a second transfer plate and weight were placed on top (load of 50 $\frac{g}{cm^2}$). The test square is left to absorb for 5 minutes; longer absorption times were evaluated but no significant differences were measured after 5 min. Then the stack of two transfer plates, test square, and the weight was lifted out of the solution and placed over a new container to drain excess liquid for 2.5 minutes. The wet test square is then weighed (W_f). We define absolute absorption in terms of an initial dry weight W_i and final wet weight W_f:

$$absorption = \frac{W_f - W_i}{W_i} \tag{3}$$

14

All measurements are made in triplicate and the average value is reported.

SEM

A Hitachi S3400N SEM operated at 5 keV was used to obtain the micrographs. The compacted fiber samples were attached to the stage using conductive carbon tape and sputter coated with Au/ Pd (60:40 ratio).

FTIR

FTIR spectra were obtained using a FTIR spectrometer (Nicolet iS50 FT/IR Spectrometer) equipped with an attenuated total reflection (ATR) unit. Spectra were recorded with a resolution of 2.0 cm^1 with 32 scans in the range of 4000 to 525 cm^{-1}. Quantitative comparison between different spectra were made using the second-derivative spectra correlation coefficient r introduced by Presterleski $et\ al.$ [75]:

$$r = \frac{\sum^N x_i y_i}{\sqrt{\sum x_i^2 \sum y_i^2}} \tag{4}$$

where x_i and y_i represent the intensity of second-derivative spectra at the ith frequency position. Spectral absorbance values in the fingerprint region between 800 and 1800 cm^{-1} were used in this calculation. Normalization of spectra is not required for this calculation. Identical spectra will return a value $r = 1.0$.

Static contact angle tensiometry

All advancing wetting measurements were made following the method described previously by Young [66]. Briefly, individual fibers were pressed between a sheet of paper and fixed in place with a small amount of adhesive. The assembly is attached to a small wire hook coupled to a sensitive electrobalance (KSV Nima, Finland). The mounted fiber is lowered slightly above a petri dish filled with distilled water. A fixed amount of water is added to immerse a portion of the fiber. The force F resulting from an increase in weight when the fiber is immersed in liquid is related to contact angle θ of the fiber by the Wilhelmy equation:

$$F = P\gamma_{LV}cos(\theta) \tag{5}$$

where P is the perimeter of the fiber and γ_{LV} is the surface tension at the liquid-vapor interface of water (72 $\mu N/m$), allowing for the determination of θ. Prior to measurement, the diameter of each fiber is first recorded in the dry state with an optical microscope and used to determine the perimeter P when calculating fiber wettability $W = F/P$. All measurements are made in triplicate and the average value is reported.

Micro-computed X-ray tomography

The 3D morphological analysis is conducted by micro-computed X-ray tomography (μCT) using an Xradia 520 Versa X-ray CT (Carl Zeiss, GmbH). Typical samples comprised 200 μg material. Contrast of samples was increased by staining with 1% aqueous KI for at least 1 h. In order to stain the blended samples while preserving their structure, these samples were freeze dried for 24 h as described above. Samples are scanned with an accelerating voltage of 80 kV and 7 W power with no filter. 1600 projects over 180° angle of rotation. The geometric magnification M_g is related to the source-to-object distance d_{so} and object-to-scintillator distance d_{os} by:

$$M_g = \frac{d_{so} + d_{os}}{d_{so}} \tag{6}$$

Large area scans were taken with a 0.4X objective and 1 s exposure with $d_{so} = 21.7\mu m$ and $d_{os} = 155.9\mu m$ fixed, giving $M_g = 8.18$. Small scan used to obtain information on individual fibers were taken with a 4X objective and 2.5 s exposure with $d_{so} = 21.7\mu m$ and $d_{os} = 50.0\mu m$ fixed, giving $M_g = 3.30$.

Life cycle assessment

A cradle-to-gate life cycle analysis was performed on sisal cellulose microfibers to quantify the materials carbon footprint. The LCA was performed according to ISO 14040 [76] using SimaPro version 8.0.

Conflict of interest

Alex Odundo is founder of Olex TechnoEnterprises which designs and manufactures sisal decorticators. The remaining authors have no competing interests to declare.

Acknowledgements

16

a TYPES OF MENSTRUAL PRODUCTS USED
(% of women)

Urban / Rural: Nigeria, Niger, Ethiopia, India, Indonesia

- Sanitary Pads
- Cloths
- Cotton Wool
- Other Materials (e.g. tampons, toilet paper, foam, natural materials)

b GDP PER CAPITA VS. ARID TO SEMI-ARID CLIMATE ZONES

- BWh Arid, desert, hot
- BWk Arid, desert, cold
- BSh Arid, steppe, hot
- BSk Arid, steppe, cold

log GDP per capita

FOREST RESOURCE DISTRIBUTION

20%	12%	9%	8%	5%	46%
Russian Federation 815 mil ha	Brazil 815 mil ha	Canada 347 mil ha	USA 310 mil ha	China 220 mil ha	Rest of the World 1870 mil ha

c Raw Plant

d Decortication — fibers / leaf

e SISAL LEAF — Cross Section

f / **g** DECORTICATED SISAL

- fiber (elementary)
- lumens
- lignin-rich fiber bundle
- perinchymal cells (removed through decortication)

MILD DELIGNIFICATION
via peroxyformic acid

MECHANICAL PROCESSING

h / **i** FLUFF PULP — delignified cellulose fibers

j Fluff Board — 10% PFA / 4% NaOH; Fluff Board — 1% PFA / 4% NaOH; Fluff Pulp; Fluff Pulp

k ABSORPTION (g/g)

- Boiled (baseline): 5.36
- Soda Pulping: 7.53
- 10% PFA 4% NaOH (blended): 23.07
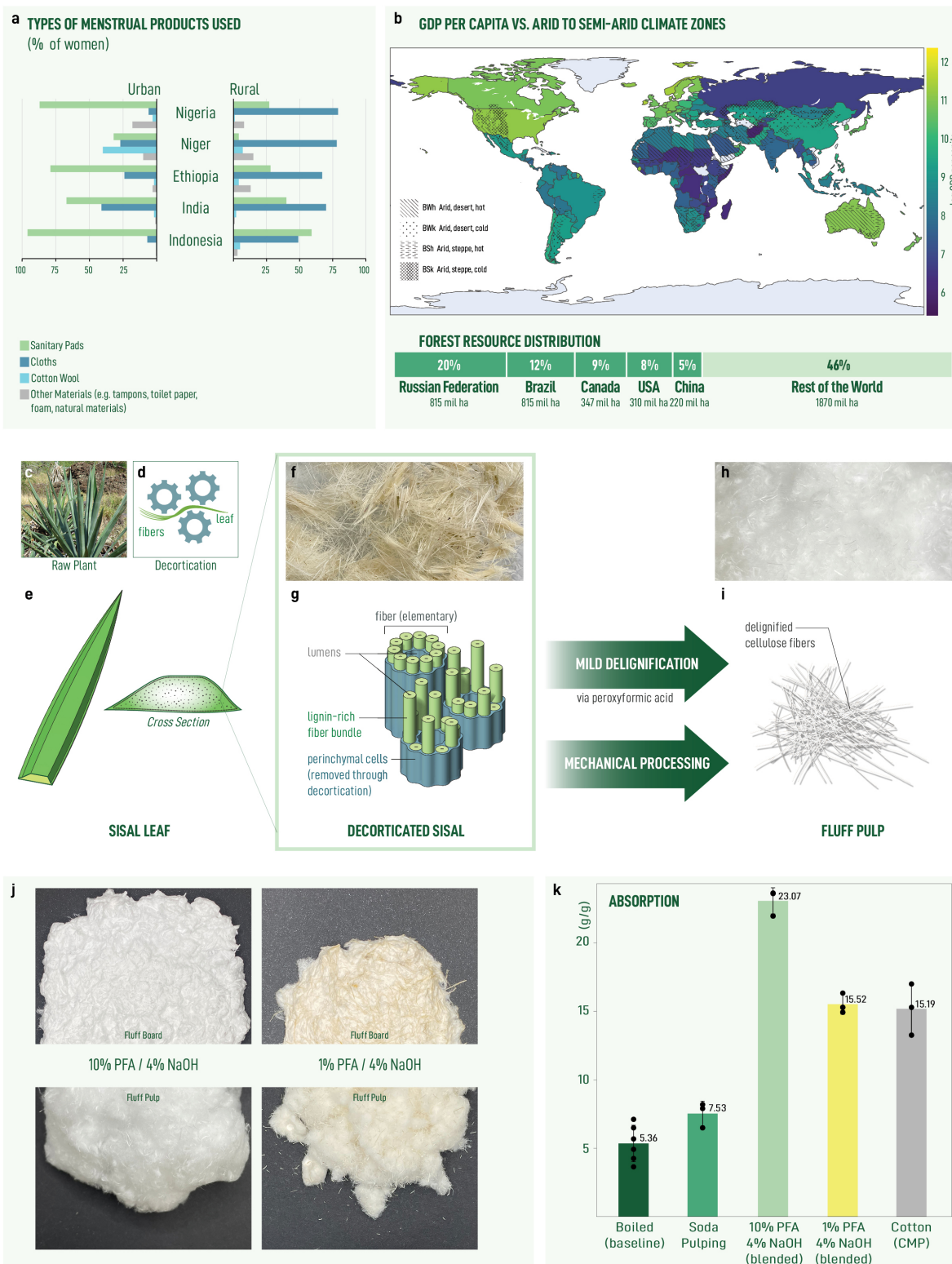- 1% PFA 4% NaOH (blended): 15.52
- Cotton (CMP): 15.19

Figure 1

18

Figure 1: Sisal as a non-wood alternative to produce absorbent material in semi-arid regions to address period poverty. [a] Preferred menstrual products in select LMICs comparing urban and rural populations with data collected from Ref [1]. [b] Low per capita GDP is coincident with arid to semi-arid climate zones. See Supplementary Notes 1 for details on panels a and b. [c] Photograph of mature sisal plant. [d] Schmeatic of mechanical decortication device. [e] Illustration showing sisal leaf and cross section. [f] Photograph of dried macrofibers obtained from leaf via decortication. [g] Schematic of decorticated macrofibers in [f] showing its hierarchical strcuture. [h] Photograph showing fluff pulp obtained from decorticated macrofibers via mild delignification via peroxyformic and mechanical treatment. [i] Illustration of fibers shown in [h]. [j] Large-scale production of fluff pulp after treatment with 10% (left) and 1% (right) peroxyformic acid. [k] Absorption performance of sisal-based materials compared with cotton-CMP.
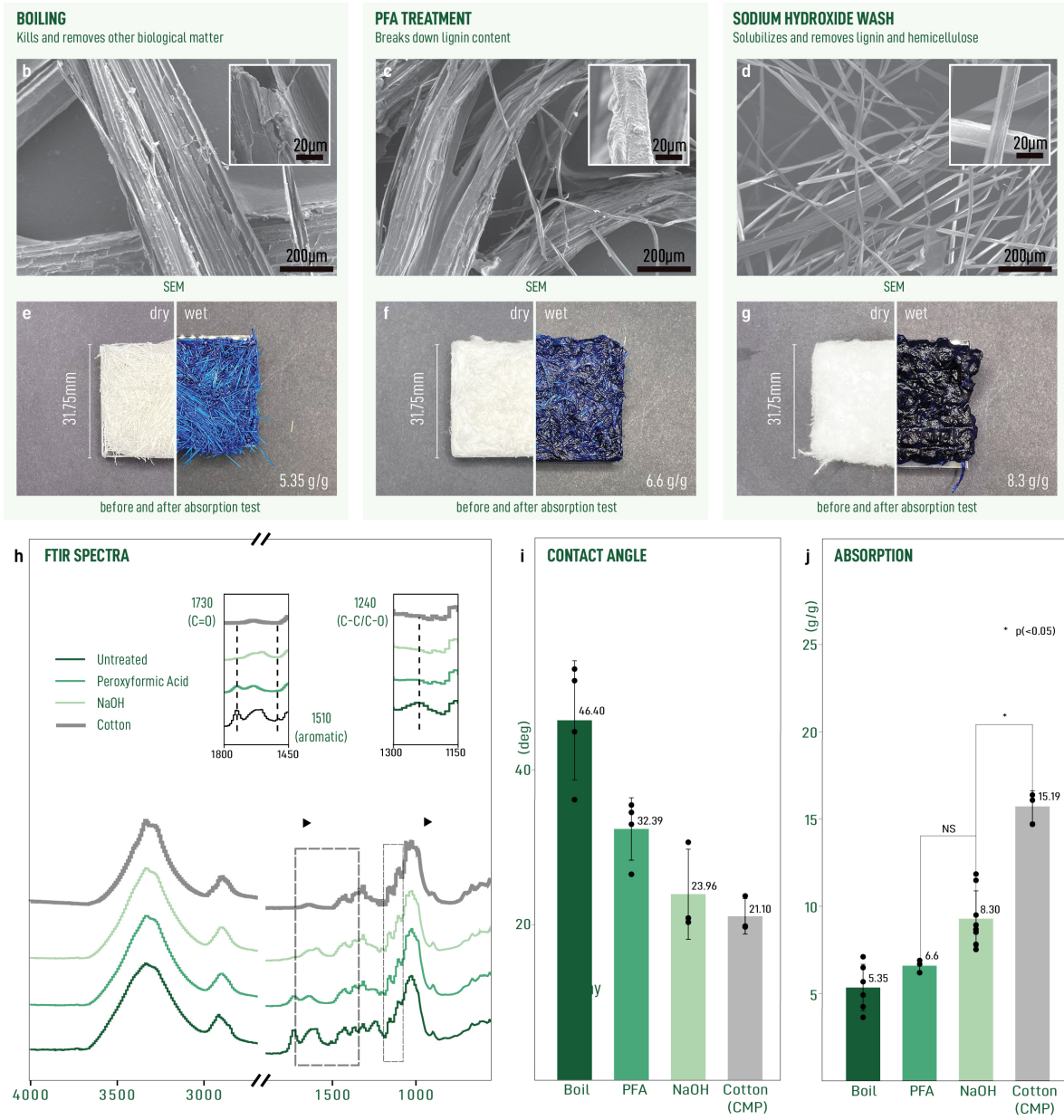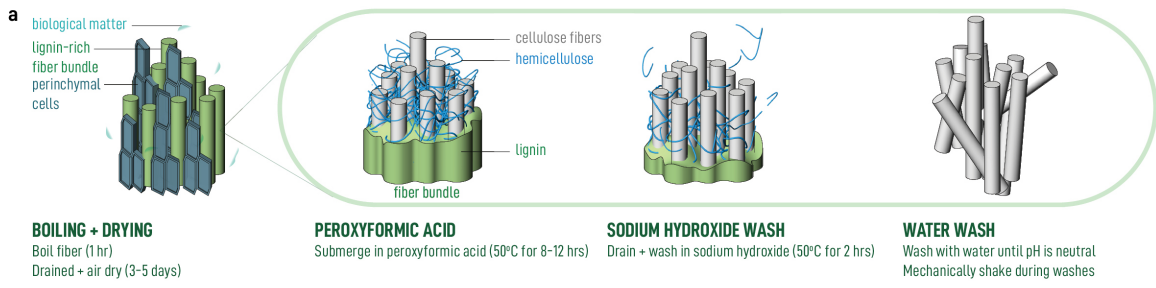
Figure 2

Figure 2: Evolution of structural and wetting properties from decorticated macrofibrers to delignified microfibers. [a] Schematic of the delignification process showing reaction of peroxyformic acid with sisal macrofibers, subsequent solubilization under alkali conditions, and debundling during aqueous wash step. SEM micrographs of fibers after boiling [b], treatment with peroxyformic acid [c], wash with sodium hydroxide and water [d]. [e-g] Photographs showing test squares prepared from [b-d] before (left) and after (right) absorption testing. The darkness of the color correlates to the amount of fluid retained by the sample. [h] FTIR spectra with important peak changes annotated in insets. [i] Advancing contact angles of individual fibers obtained from static contact angle tensiometry. [j] Absorption performance for test squares prepared from fibers. Student's t-test P value > 0.05, NS (not significant); *P value < 0.05.

a WET PULP — Post PFA treatment, NaOH wash, water wash → AIR DRYING → FLUFF BOARD → DRY BLENDING → FLUFF PULP

b ABSORPTION — liquid uptake + retention

c ABSORPTION (g/g)

Air Dry No Blend: 9.64
Air Dry 45s Blend: 19.79
Air Dry 300s Blend: 23.93
Freeze Dry: 12.96
Cotton (CMP): 15.19

d ABSORPTION VS. POROSITY

- 10% PFA, 4% NaOH, Freeze dried
- 10% PFA, 4% NaOH, Air dried (no blend)
- 10% PFA, 4% NaOH, Air dried (w/ blend)
- 1% PFA, 4% NaOH, Air dried (w/ blend)
- Cotton (CMP)

Porosity axis: 0.75, 0.8, 0.85, 0.9, 0.95

10% PFA / 4% NaOH — no dry blending

10% PFA / 4% NaOH — 45 seconds of dry blending

1% PFA / 4% NaOH — 45 seconds of dry blending

e 5mm **f** 5mm **g** 5mm

h SEM — 1mm **i** SEM — 1mm **j** SEM — 1mm

CT scan – 2D slice — 500 µm (×3)

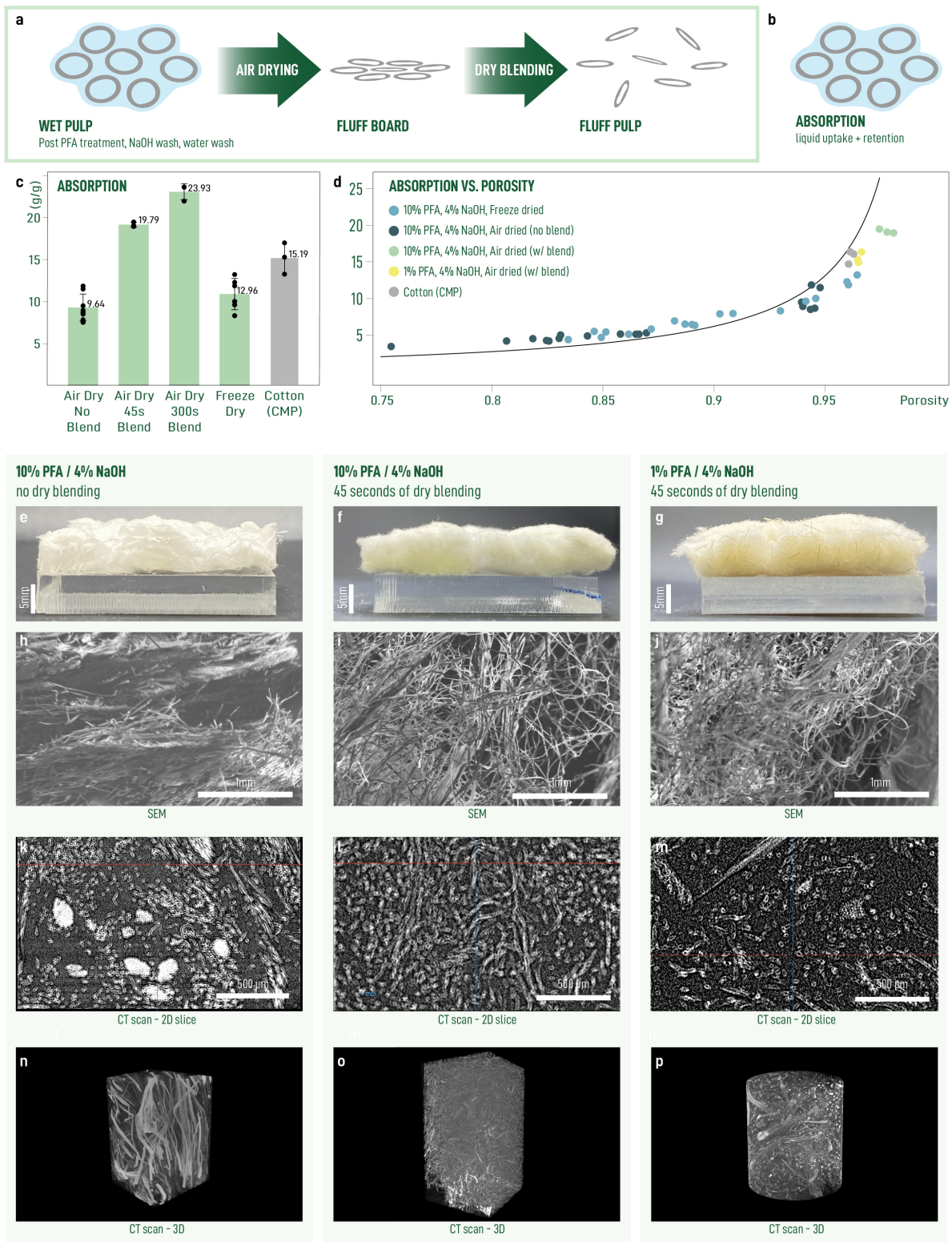**n** CT scan – 3D **o** CT scan – 3D **p** CT scan – 3D

Figure 3

22

Figure 3: Increasing absorption capacity through mechanical processing. [a] Schematic showing collapse of network during drying and subsequent debonding of collapsed network into porous fluff pulp. [b] Schematic showing how debonding correlates with liquid uptake and retention. The extent of debonding depends on the duration of dry blending. [c] Absorption capacity for test squares prepared from samples subject to different processes of drying and mechanical treatment. [d] Absorption capacity for test squares with the black curve showing the theoretical absorption capacity as a function of porosity. Photographs showing cross-section of test squares for 10% perfooxyfomic-acid treated, air dried, unblended [e], 10% perfooxyfomic-acid treated, air dried, blended (45 s) [f], 1% perfooxyfomic-acid treated, air dried, blended [g]. SEM micrographs [h-j], μCT cross sections [k-m], and reconstructed 3D volumes [n-p] of samples shown in [e-g], respectively.
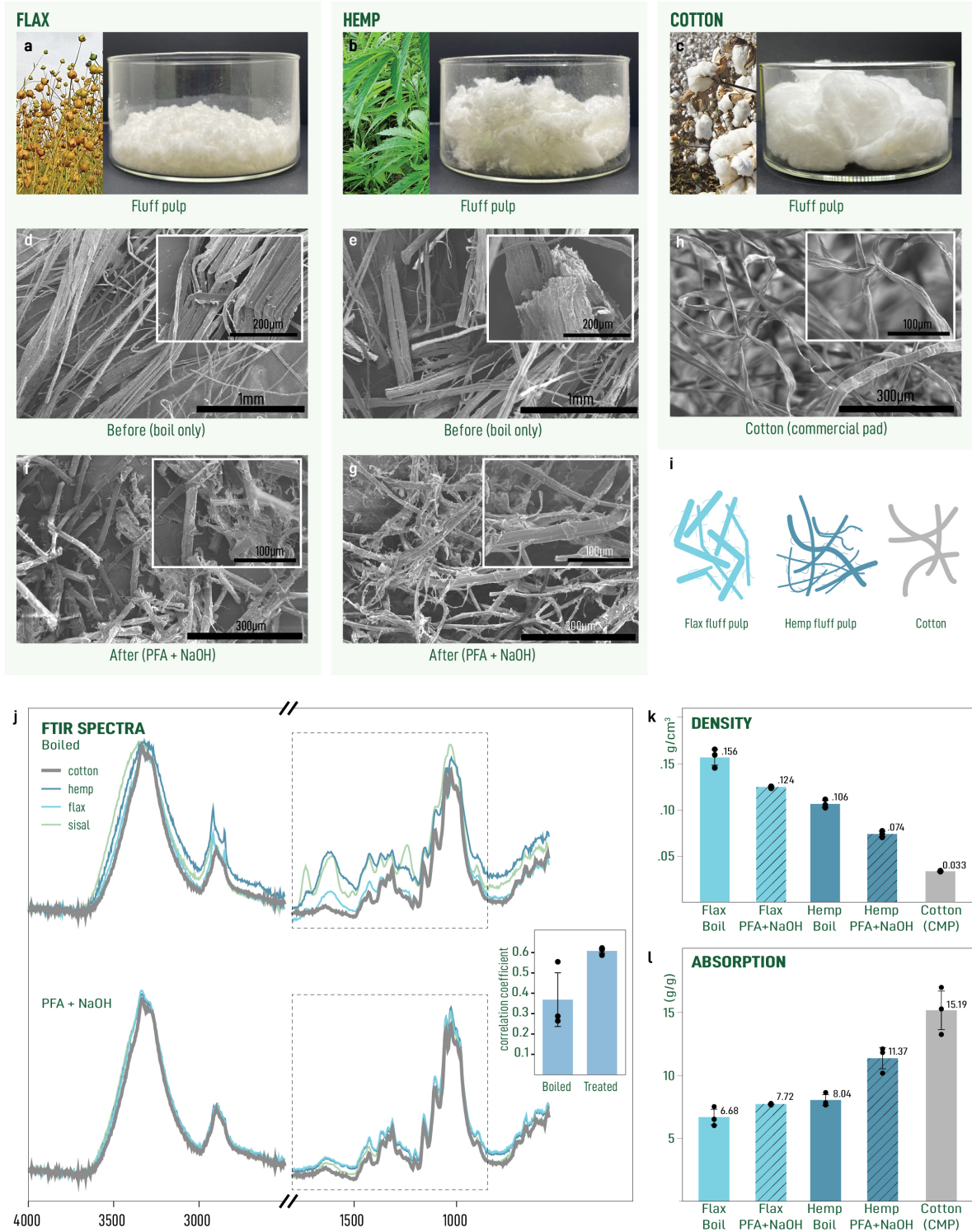
High porosity (Flax)   Low porosity (Cotton)

FLAX

a

Fluff pulp

d

200μm

1mm

Before (boil only)

f

100μm

300μm

After (PFA + NaOH)

HEMP

b

Fluff pulp

e

200μm

1mm

Before (boil only)

g

100μm

300μm

After (PFA + NaOH)

COTTON

c

Fluff pulp

h

100μm

300μm

Cotton (commercial pad)

i

Flax fluff pulp   Hemp fluff pulp   Cotton

j FTIR SPECTRA
Boiled
— cotton
— hemp
— flax
— sisal

PFA + NaOH

4000   3500   3000   1500   1000

correlation coefficient: Boiled, Treated

k DENSITY

.15   .156
.10   .124   .106
.05   .074   0.033

Flax Boil | Flax PFA+NaOH | Hemp Boil | Hemp PFA+NaOH | Cotton (CMP)

l ABSORPTION

15   15.19
      11.37
10   8.04
5   6.68   7.72

Flax Boil | Flax PFA+NaOH | Hemp Boil | Hemp PFA+NaOH | Cotton (CMP)

Figure 4

24

Figure 4: Morphology of single fibers from different fiber-rich plants effects absorption capacity. Photographs of large-scale production of fluff pulps from flax [a], hemp macrofibers [b], and collected CCMP [c]. SEM micrograps of boiled macrofibers [d and e] and fluff pulps (45 s dry blended) [f and g] obtained from flax and hemp, respectively. [h] SEM micrograph showing collected CCMP. [i] Illustration highlighting the key morphological features of the fluff pulp and CCMP fibers. [j] FTIR spectra comparing boiled macrofibers (top) with fluff pulp microfibers (bottom). Inset shows spectral correlation coeffcient for each fiber type referenced against CCMP. Densities [k] and absorption capacity [l] of test squares squares.
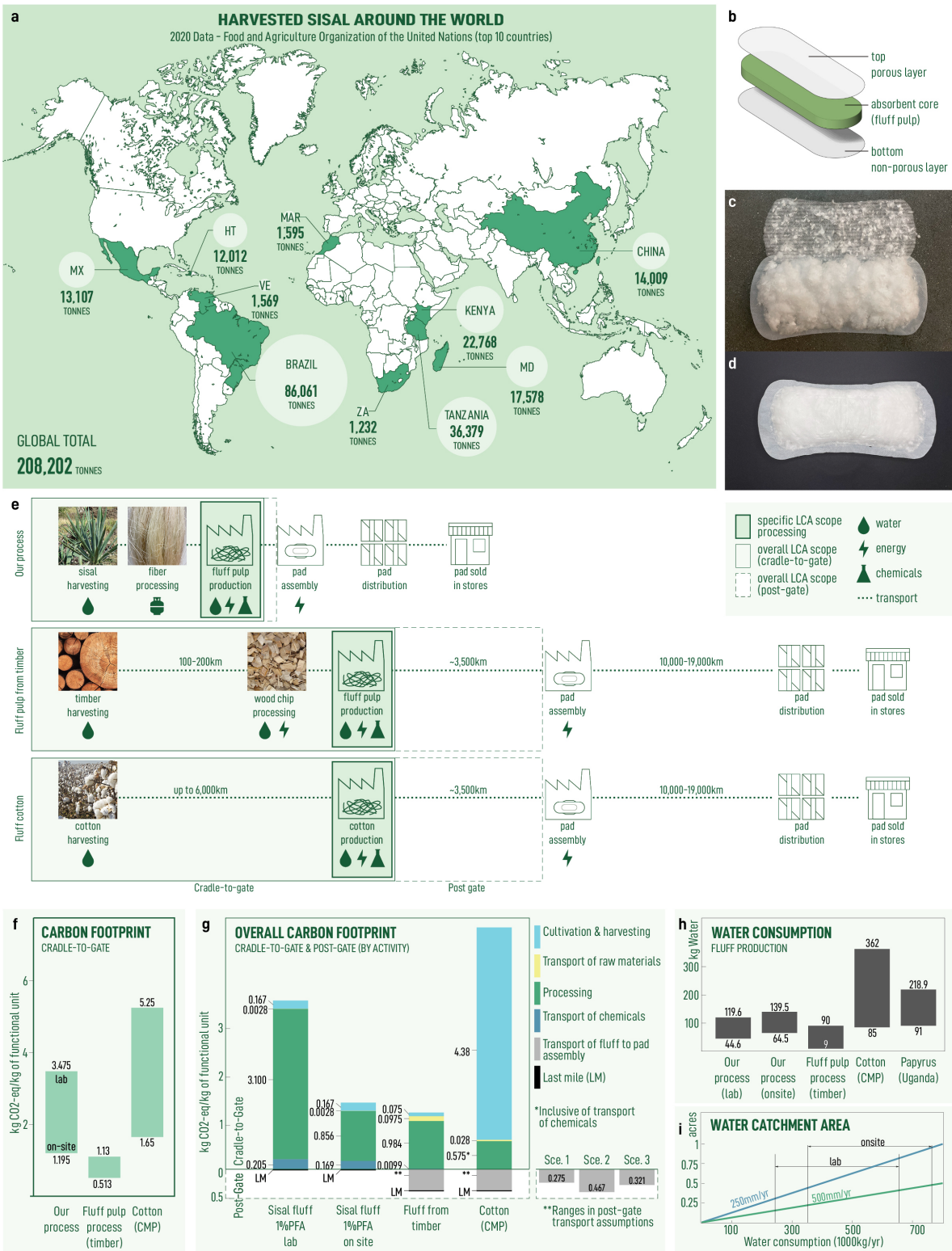
Figure 5

Figure 5: Life-cycle analysis of sisal fluff pulp production in the context of distributed manufacturing of menstrual pads in semi-arid regions. [a] Geographic distribution of the 10 largest nations producing sisal based on data obtained from the FAO [68]. [b] Schematic showing assembly of a three-layer menstrual pad. Photographs showing sisal fluff pulp incorporated [c] into an assembled three-layer pad [d]. The other two layers are obtained from a commercially available menstrual pad. [e] Schematic showing activities described in life-cycle analysis with boxes defining the activities within each scope of the analysis. [f] Carbon footprint analysis of fluff production with comparison to common alternatives (wood-derived fluff pulp and cotton). Upper and lower bounds for our process correspond to lab and on-site production strategies, respectively; for common alternatives, these bounds are defined by values obtained from literature. [g] Carbon footprint analysis showing contribution by activity with cradle-to-gate and post-gate scopes. **Represents the 3 post-gate transportation scenarios considered (see Supplementary Note 6). [h] Water consumption associated with fluff production. [i] Water catchment area required to support production dependent on annual rainfall assumptions for arid and semi-arid regions (see Supplemental Note 8).

References

[1] Amaya, L., Marcatili, J. & Bhavaraju, N. *Advancing Gender Equity by Improving Menstrual Health: Opportunities in Menstrual Health and Hygiene* (FSG, 2020).

[2] Programme, W. J. M. Progress on household drinking water, sanitation and hygiene. 2000-2020 92–97 (2020).

[3] Harrison, M. E. & Tyson, N. Menstruation: Environmental impact and need for global health equity. *International Journal of Gynecology Obstetrics* **160**, 378–282 (2022).

[4] Gupta, A. *Design of an absorbent and comfortable sanitary napkin for applications in developing countries* (Thesis: S.B., Massachusetts Institute of Technology, Department of Materials Science and Engineering, 2014).

[5] Mujinja, P. G., Mackintosh, M., Justin-Temu, M. & Wuyts, M. Local production of pharmaceuticals in africa and access to essential medicines: 'urban bias' in access to imported medicines in tanzania and its policy implications. *Globalization and Health* **10** (2014).

[6] Schmitz, H. Growth constraints on small-scale manufacturing in developing countries: a critical review. *World Development* **10**, 429–450 (1982).

[7] Musaazi, M. K. & et al. Quantification of social equity in life cycle assessment for increased sustainable production of sanitary products in uganda. *Journal of Cleaner Production* **96**, 569–579 (2015).

[8] Babiker, A. A. The role of rural industries in the arid and semi-arid areas of the sudan. *GeoJournal* **6**, 49–55 (1982).

[9] Kumar, M. J. Is india going to be a major hub of semiconductor chip manufacturing? *IETE Technical Review* **38**, 279–281 (2021).

[10] Fourcassier, S., Douziech, M., Pérez-López, P. & Schiebinger, L. Menstrual products: A comparable life cycle assessment. *Cleaner Environmental Systems* **7**, 100096 (2022).

[11] Ching, T. W. & et al. Microwave-assisted hydrothermal decomposition of super absorbent polymers. *ACS Sustainable Chemistry Engineering* **8**, 14504–14510 (2020).

[12] Hand, J., Hwang, C., Vogel, W., Lopez, C. & Hwang, S. An exploration of market organic sanitary products for improving menstrual health and environmental impact. *Journal of Water, Sanitation and Hygiene for Development* **13**, 63–77 (2023).

[13] Sasidaran, S. & et al. Physical properties of menstrual hygiene waste as feedstock for onsite disposal technologies. *Journal of Water, Sanitation and Hygiene for Development* **11**, 474–482 (2021).

[14] Li, T. & et al. Developing fibrillated cellulose as a sustainable technological material. *Nature* **590**, 47–56 (2021).

[15] Crowther, T. W. & et al. Mapping tree density at a global scale. *Nature* **525**, 201–205 (2015).

[16] Buitrago-Tello, R., Venditti, R. A., Jameel, H., Yao, Y. & Echeverria, D. Carbon footprint of bleached softwood fluff pulp: Detailed process simulation and environmental life cycle assessment to understand carbon emissions. *ACS Sustainable Chemistry Engineering* **10**, 9029–9040 (2022).

[17] Börjesson, M. H. & Ahlgren, E. O. *Technology Brief I07: Pulp and Paper Industry* (International Energy Agency - Energy Technology Systems Analysis Program, 2015). URL https://iea-etsap.org/E-TechDS/PDF/I07$_PulpPaper_May$2015$OK.pdf$.

[18] Kindelan, K. Stores report tampon, menstrual pad shortage as women struggle to find product (2022). URL https://abc7ny.com/tampon-shortage-2022-tampons-period-products-pad/11961756/.

[19] Molina, A. & et al. Low cost centrifugal melt spinning for distributed manufacturing of non-woven media. *PLOS ONE* **17**, e0264933 (2022).

[20] Abd El-Sayed, E. S., El-Sakhawy, M. & El-Sakhawy, M. A.-M. Non-wood fibers as raw material for pulp and paper industry. *Nordic Pulp Paper Research Journal* **35**, 215–230 (2020).

[21] Favero, A., Thomas, V. M. & Luettgen, C. O. Life cycle analyses of alternative fibers for paper. *Journal of Advanced Manufacturing and Processing* **1** (2019).

[22] Ferdous, T., Ni, Y., Quaiyyum, M. A., Uddin, M. N. & Jahan, M. S. Non-wood fibers: Relationships of fiber properties with pulp properties. *ACS Omega* **6**, 21613–21622 (2021).

[23] Ferdous, T., Jahan, M. S., Quaiyyum, M. A. & Uddin, M. N. Formic acid pulping of crops residues available in bangladesh. *Biomass Conversion and Biorefinery* **10**, 289–297 (2019).

[24] Rebola, S. M., Ferreira, J. & Evtuguin, D. V. Potential of bleached eucalyptus kraft pulp for applications in nonwoven fibrous fabrics. *Journal of Engineered Fibers and Fabrics* **15** (2020).

[25] Azevedo, C. A., Rebola, S. M. C., Domingues, E. M., Figueiredo, F. M. L. & Evtuguin, D. V. Relationship between surface properties and fiber network parameters of eucalyptus kraft pulps and their absorption capacity. *Surfaces* **3**, 265–281 (2020).

[26] Practical Action, The Schumacher Centre for Technology and Development. *Small-scale papermaking.*

[27] Leidy, J. The parasites of the termites. *J. Acad. Nat. Sci. (Phila.)* **8**, 425–447 (1881).

[28] Kracher, D. & et al. Extracellular electron transfer systems fuel cellulose oxidative degradation. *Science* **352**, 1098–1101 (2016).

[29] Wood, P. M. Pathways for production of fenton's reagent by wood-rotting fungi. *FEMS Microbiology Reviews* **13**, 313–320 (1994).

[30] Brune, A. Symbiotic digestion of lignocellulose in termite guts. *Nature Reviews Microbiology* **12**, 168–180 (2014).

[31] Haverty, D., Dussan, K., Piterina, A. V., Leahy, J. J. & Hayes, M. H. B. Autothermal, single-stage, performic acid pretreatment of miscanthus x giganteus for the rapid fractionation of its biomass components into a lignin/hemicellulose-rich liquor and a cellulase-digestible pulp. *Bioresource Technology* **109**, 173–177 (2012).

[32] Ragazzo, P., Chiucchini, N., Piccolo, V. & Ostoich, M. A new disinfection system for wastewater treatment: performic acid full-scale trial evaluations. *Water Science and Technology* **67**, 2476–2487 (2013).

[33] Xu, J. & et al. Organic wastewater treatment by a single-atom catalyst and electrolytically produced h2o2. *Nature Sustainability* **4**, 233–241 (2020).

[34] Echeverria, D., Venditti, R., Jameel, H. & Yao, Y. A general life cycle assessment framework for sustainable bleaching: A case study of peracetic acid bleaching of wood pulp. *Journal of Cleaner Production* **290**, 125854 (2021).

[35] Cai, M., Sun, P., Zhang, L. & Huang, C.-H. Uv/peracetic acid for degradation of pharmaceuticals and reactive species evaluation. *Environmental Science Technology* **51**, 14217–14224 (2017).

[36] Sun, P. & et al. Rapid disinfection by peracetic acid combined with uv irradiation. *Environmental Science amp; Technology Letters* **5**, 400–404 (2018).

[37] Santacesaria, E., Russo, V., Tesser, R., Turco, R. & Di Serio, M. Kinetics of performic acid synthesis and decomposition. *Industrial Engineering Chemistry Research* **56**, 12940–12952 (2017).

[38] Bi, Z., Lai, B., Zhao, Y. & Yan, L. Fast disassembly of lignocellulosic biomass to lignin and sugars by molten salt hydrate at low temperature for overall biorefinery. *ACS Omega* **3**, 2984–2993 (2018).

[39] Xia, Q. & et al. A strong, biodegradable and recyclable lignocellulosic bioplastic. *Nature Sustainability* **4**, 627–635 (2021).

[40] Rousu, P., Rousu, P. & Anttila, J. Sustainable pulp production from agricultural waste. *Resources, Conservation and Recycling* **35**, 85–103 (2002).

[41] Lewis, R. J. & Hutchings, G. J. Recent advances in the direct synthesis of hydrogen peroxide. *ChemCatChem* **11**, 298–308 (2018).

[42] Lust, D. *et al.* Decentralized city district hydrogen storage system based on the electrochemical reduction of carbon dioxide to formate. In *Proceedings of the 13th International Renewable Energy Storage Conference 2019 (IRES 2019)*, 137–144 (Atlantis Press, 2019/11). URL https://www.atlantis-press.com/article/125923326.

[43] Wang, Q. & et al. Molecularly engineered photocatalyst sheet for scalable solar formate production from carbon dioxide and water. *Nature Energy* **5**, 703–710 (2020).

[44] Thijs, B., Rongé, J. & Martens, J. A. Matching emerging formic acid synthesis processes with application requirements. *Green Chemistry* **24**, 2287–2295 (2022).

[45] Scharpf, E. *et al.* Highly absorbent and retentive fiber material (U.S. Patent 9365972B2, 2014).

[46] Bothra, T., Kane, G., Saigal, A. & Kagetsu, K. Absorbent article having natural fibers (U.S. Patent 10,736,790 B2, 2020).

[47] Raya, F. T. & et al. Extreme physiology: Biomass and transcriptional profiling of three abandoned agave cultivars. *Industrial Crops and Products* **172**, 114043 (2021).

[48] Kimaro, M. B. M. . T. Y., D. Review of sisal production and research in tanzania. *African Study Monographs* **15**, 227–242 (1994).

[49] Hartemink, A. E. & Kekem, A. J. Nutrient depletion in ferralsols under hybrid sisal cultivation in tanzania. *Soil Use and Management* **10**, 103–107 (1994).

[50] Borland, A. M., Griffiths, H., Hartwell, J. & Smith, J. A. C. Exploiting the potential of plants with crassulacean acid metabolism for bioenergy production on marginal lands. *Journal of Experimental Botany* **60**, 2879–2896 (2009).

[51] Chatterjee, P. K. & Gupta, B. S. *Absorbent Technology. Chapter 1: porous Structure and Liquid Flow Models* (Elsevier, 2002).

[52] Bureau of Indian Standards. *IS 5405: Sanitary Napkins* (1980). URL https://archive.org/details/gov.in.is.5405.1980.

[53] Carter, H. R. The decortication of fibrous plants, with special reference to the belgian flax industry. *Journal of the Textile Institute* **4**, 231–265 (1913).

31

[54] Tahir, P., Ahmed, A., SaifulAzry, S. & Ahmed, Z. Retting process of some bast plant fibres and its effect on fibre quality: a review. *BioResources* **6** (2011).

[55] Melelli, A., Jamme, F., Beaugrand, J. & Bourmaud, A. Evolution of the ultrastructure and polysaccharide composition of flax fibres over time: When history meets science. *Carbohydrate Polymers* **291**, 119584 (2022).

[56] Perez, D. d. S. & et al. Peroxyformic acid pulping of eucalyptus grandis wood chips and sugar cane bagasse in one stage and characterization of the isolated lignins. *Journal of Wood Chemistry and Technology* **18**, 333–365 (1998).

[57] Li, Z. & et al. Sustainable high-strength macrofibres extracted from natural bamboo. *Nature Sustainability* **5**, 235–244 (2021).

[58] *Methods in Lignin Chemistry.* (Springer, Berlin-Heidelberg, Germany, 1992).

[59] Deuss, P. J. & et al. Aromatic monomers by in situ conversion of reactive intermediates in the acid-catalyzed depolymerization of lignin. *Journal of the American Chemical Society* **137**, 7456–7467 (2015).

[60] More, A., Elder, T. & Jiang, Z. A review of lignin hydrogen peroxide oxidation chemistry with emphasis on aromatic aldehydes and acids. *Holzforschung* **75**, 806–823 (2021).

[61] Bailey, R. W. & Pickmere, S. E. Alkali solubility of hemicelluloses in relation to delignification. *Phytochemistry* **361**, 501–504 (1975).

[62] Barkakaty, B. C. Some structural aspects of sisal fibers. *Journal of Applied Polymer Science* **20**, 2921–2940 (1976).

[63] Kubo, S. & Kadla, J. F. . Hydrogen bonding in lignin: a fourier transform infrared model compound study. *Biomacromolecules* **6**, 2815–2821 (2005).

[64] Fumoto, E. & et al. Determination of carbonyl functional groups in lignin-derived fraction using infrared spectroscopy. *Fuel* **318**, 123530 (2022).

[65] McCall, E. R. & Jurgens, J. F. Chemical composition of cotton. *Textile Research Journal* **21**, 19–21 (1951).

[66] Young, R. Wettability of wood pulp fibers: Applicability of methodology. *Wood Fiber Science* **8**, 120–128 (1976).

[67] Barsberg, S. & Thygesen, L. G. Nonequilibrium phenomena influencing the wetting behavior of plant fibers. *Journal of Colloid and Interface Science* **234**, 59–67 (2001).

[68] Food & of the United Nations, A. O. Crops and livestock products: Sisal, raw (2021). Data retrieved from FAO.org in April 2023, `https://www.fao.org/faostat/en/data/QCL/visualize`.

[69] Hurter, R. Tcf bleached sisal market pulp: potential reinforcing fibre for commodity papers - part 2. *Proceedings of TAPPI Pulping Conference* **2**, 655–665 (1997).

[70] Cantalino, A., Torres, E. A. & Silva, M. S. Sustainability of sisal cultivation in brazil using co-products and wastes. *Journal of Agricultural Science* **7** (2015).

[71] HP Now. *Technical Datasheet: HP Gen A series* (2022). Technical details for the second generation series were shared with the authors by personal correspondence with HP Now.

[72] Olsson, H. D., J. & Pålsson, H. Framework of last mile logistics research: A systematic review of the literature. *Sustainability* **11**, 7131 (2019).

[73] Stathatou, P., Garmulewicz, L., Corbin, L., Bolumburu, P. & Kremer, Z. *Biomaterials and Regenerative Agriculture: Linkages and Opportunities. The Case of the Greak Lakes Region, Michigan.* (Materiom, 2022).

[74] Lan, K. & et al. Techno-economic analysis of decentralized preprocessing systems for fast pyrolysis biorefineries with blended feedstocks in the southeastern united states. *Renewable and Sustainable Energy Reviews* **143**, 110881 (2021).

[75] Prestrelski, S. J., Tedeschi, N., Arakawa, T. & Carpenter, J. F. Dehydration-induced conformational transitions in proteins and their inhibition by stabilizers. *Biophysical Journal* **65**, 661–671 (1993).

[76] International Standards Organization. *ISO 14040:2006 Environmental Management—Life Cycle Assessment— Principles and Framework* (2006). URL `https://archive.org/details/gov.in.is.5405.1980`.